Title

Dynamic Boundary Layer Simulation of Pulsed CO2 Electrolysis on a Copper Catalyst

Journal

ACS Energy Letters, 6(4)

ISSN

2380-8195

Authors

Bui, Justin C
Kim, Chanyeon
Weber, Adam Z
et al.

Publication Date

2021

DOI

10.1021/acsenergylett.1c00364

Dynamic Boundary Layer Simulation of Pulsed CO_2 Electrolysis on a Copper Catalyst

Justin C. Bui[1,2], Chanyeon Kim[1,2], Adam Z. Weber[2], and Alexis T. Bell[1,2]*

[1] Department of Chemical and Biomolecular Engineering
University of California Berkeley
Berkeley, CA 94720, USA

[2] Joint Center for Artificial Photosynthesis
Lawrence Berkeley National Laboratory
Berkeley, CA 94720, USA

ACS Energy Letters
March 4, 2021

***Corresponding Author**
email: alexbell@berkeley.edu
phone: (510) 642-1536

Abstract

Pulsed electrolysis has been demonstrated to improve the FE to C_{2+} products during the electrochemical reduction of CO_2 over a Cu catalyst, but the nature of this enhancement is poorly understood. Herein, we develop a time-dependent continuum model of pulsed CO_2 electrolysis on Cu in 0.1 M $CsHCO_3$ that faithfully represents the experimentally observed effects of pulsed electrolysis. This work shows that pulsing results in dynamic changes in the pH and CO_2 concentration near the Cu surface, which lead to an enhanced C_{2+} FE as a consequence of repeatedly accessing a transient state of heightened pH and CO_2 concentration at high cathodic overpotential. Using these insights, a variety of pulse shapes are explored to establish operating conditions that maximize the rate of C_{2+} product formation and minimize the rates of H_2 and C_1 product formation.

Electrochemical carbon dioxide reduction (CO_2R) holds considerable potential for using renewably sourced electricity (wind and solar) to convert CO_2 to valuable chemicals and fuels.[1–3] Of the catalysts explored for this process, copper (Cu)-containing materials are uniquely capable of catalyzing CO_2R with high faradaic efficiency (FE) to C_{2+} products.[3–5] These findings have motivated efforts aimed at enhancing the C_{2+} FE.[5,6]

Recent studies have demonstrated that the microenvironment surrounding the Cu catalyst plays a significant role in dictating FE; therefore, developing an understanding of the impacts of microenvironment is critical to guiding improvements in performance.[4,5,7,8] For instance, because the current density for C_1 products is depressed at high pH, increasing the pH near the cathode surface leads to improvements in C_{2+} FE.[4,5,9–12] Additionally, increasing local CO_2 concentration increases current density for CO_2R and suppresses the H_2 evolution reaction (HER).[5,13,14] It has also been demonstrated that films of an organic material or ionic liquids in contact with the catalyst enhance the FE to C_{2+} products through control of mass transfer and/or stabilization of intermediates to these products.[15–17] Lastly, the use of tandem bi-metallic catalysts, e.g., Ag-Cu, can contribute to higher concentrations of adsorbed intermediates, enhancing C_{2+} FE.[18]

Another method for enhancing C_{2+} FE is pulsed electrolysis.[19–26] In this case, the cathode potential is alternated between a more and less cathodic potential. The more cathodic potential is typically near -1.0 V vs RHE, whereas values of the less cathodic potential range between -0.8 to +0.4 V vs RHE. When the less cathodic potential is above +0.4 V vs RHE, periodic oxidation and reduction of Cu restructures the Cu surface.[21] Kim *et al.*[21] have reported the pulsed electrolysis of CO_2 in 0.1 M $CsHCO_3$, using a pulse sequence of 10 s periods between cathodic voltages of -0.8 and -1.15 V vs RHE. Their work showed that the C_{2+} FE and total current density increased upon pulsing. To interpret these data, the authors simulated variations in the surface

pH and CO_2 concentration given the experimentally measured current density.[21] They then proposed that the enhanced concentration of CO_2 during pulsed electrolysis was responsible for the enhancement in C_{2+} product formation. Since their model did not include the effects of pH and CO_2 concentration on the kinetics for forming individual products, they were unable to assess the influence of these parameters. In this study, we describe a continuum model of the CO_2R boundary layer that overcomes these shortcomings and provides quantitative information about the influence of pulsed electrolysis on C_{2+} FE and current density, proposing that a transient state of heightened pH, CO_2 concentration and driving potential are responsible for improved CO_2R.[15] The dynamic model reported here is also used to optimize pulse shape to maximize C_{2+} FE.

Figure 1A illustrates the 1-D model. It consists of a Cu electrode and the associated 100 μm thick mass-transport boundary layer. Model details are given in **Section S1** of the SI. A time-dependent Dirichlet boundary condition is used at the Cu surface to describe the applied rectangular-wave potential. The pulse shape for most of the simulations is that employed by Kim *et al*.[21] A Neumann boundary condition is applied for species flux at the Cu surface as described using Butler-Volmer kinetics (see **Section S2**).[27] At the outer boundary, the concentration of all species is defined by bulk concentrations in 0.1 M $CsHCO_3$, assuming that the CO_2 concentration is given by Henry's Law at 1 atm pressure and 25°C (34 mM).[28] The equations representing the model were solved in COMSOL Multiphysics 5.5 (see **Section S3** for computational methods).

The results of the simulation are depicted in **Figure 1**. As seen in **Figure 1B**, the simulated product FEs are quite consistent with the experimental data of Kim et al.[21] In this work, pulsed electrolysis is compared to static electrolysis at the same time-averaged potential, because these

two scenarios represent identical voltage efficiency (defined as the standard reduction potential divided by the applied cathodic potential). This efficiency metric is chosen primarily for simplicity of comparing modeled results of pulsed electrolysis with various pulse shapes to those of static electrolysis. However, future studies should aim to utilize more sophisticated power-based efficiency metrics for transient systems. The simulation shows that pulsing improves the FE for C_{2+} products from 42 to 65%, and the total current density from 6.22 to 7.98 mA cm^{-2}. These results are consistent with experiments, which show that the FE for C_{2+} products is enhanced from 48 to 80%, and the current density increases from 7.20 to 8.10 mA cm^{-2}.

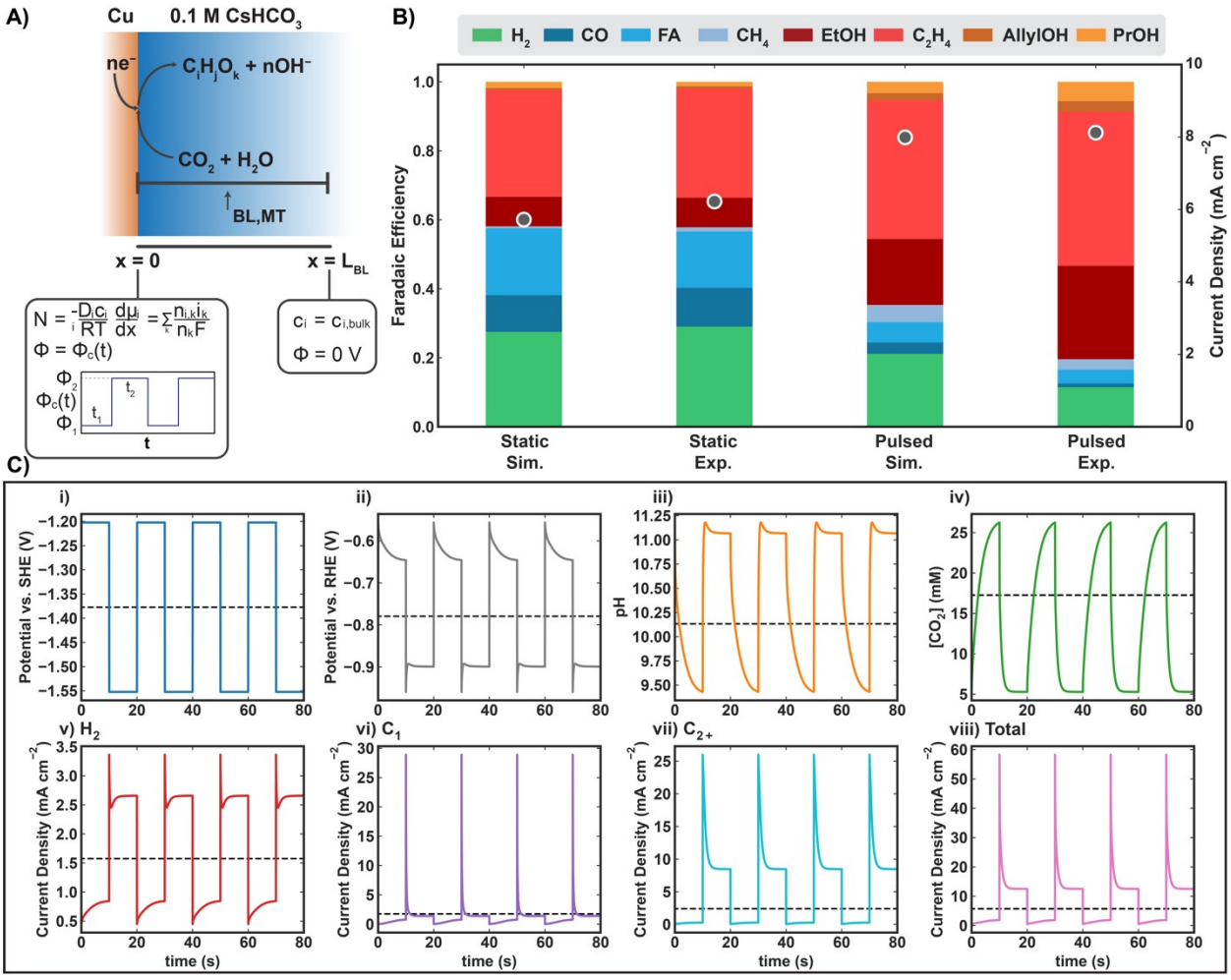

Figure 1: **(A)** Schematic representation of the boundary-layer model and boundary conditions. **(B)** Comparison of the product FEs (stacked bars) and total current densities (markers) observed experimentally[21] and those determined from simulations of both static and pulsed electrolysis. For static electrolysis, the product FEs shown represent static electrolysis at the time averaged potential of −1.37 V vs. SHE. Pulsed electrolysis is conducted using a rectangular voltage waveform between −1.20 V vs SHE (Φ_1) and −1.55 V vs SHE (Φ_2), with 10 s holds at each voltage (t_1, t_2). Experimental FEs are normalized to a total of 1. **(C)** Overview of simulated pulsed CO_2R. **(i)** Applied cathodic potential on an SHE scale, **(ii)** cathodic potential on an RHE scale, **(iii)** surface pH, and **(iv)** surface CO_2 concentration. **(v)** Partial current density due to H_2, **(vi)** C_1 products, and **(vii)** C_{2+} products. **(viii)** Total current density. Dashed lines represent values for a static applied potential at the time-average potential.

The time-dependent profiles depicted in **Figure 1C** demonstrate further consistency with experimental results. The CO_2 profile is quite similar to that measured by differential electrochemical mass spectrometry reported by Kim *et al.* **(Figure S3)**, and the pH profile matches their original simulation.[21] Since all of the surface reactions generate OH^- anions at a molar rate equivalent to that of charge passed through the electrode,[29–31] the surface pH increases as the applied overpotential and current density increase. Conversely, due to increased consumption of CO_2 at higher overpotentials, the local CO_2 concentration decreases. The time-dependent profiles of the surface concentrations of electrolyte ions (**Figure S4**) reveal that at the higher currents where pH is enhanced, the local buffer equilibria shift heavily towards CO_3^{2-}, which in turn decreases the local CO_2 concentration and increases the concentration of Cs^+ at the surface due to the enforcement of electroneutrality in the simulation.[10] Lastly, it has been reported that the FE for C_{2+} products dominates at higher applied potentials and that the FEs for C_1 products and H_2 dominate at lower applied potentials.[4,32] The model presented captures these trends very effectively.

We note, however, that there are discrepancies between the pulsed simulations and experimental behavior. First, the transient spikes in total current density observed experimentally (**Figure S3a**) were less pronounced because the data acquisition time was 1 s.[21] When the data

acquisition time was decreased to 0.2 ms, the peaks were enhanced (**Figure S3b**). The time-dependent CO_2 concentration profile (**Figure S3c**) is also consistent with those simulated, but the concentration swings are slightly less severe. These discrepancies in the CO_2 peaks can be attributed to the inability of the potentiostat to perform perfect step changes, the 1-s acquisition time of the differential electrochemical mass spectrometry, or the omission of double-layer formation from the model.[9] The time constant for the double-layer charging is approximately 6-30 ms,[21,33] and during that period, current would be dominated by double-layer charging as opposed to CO_2R, mitigating the peaks simulated. To capture fully these effects, requires a molecular-scale representation of the electrolyte double-layer, which is beyond the scope of the current work. While the exact values for simulated C_{2+} FE and total current density differ slightly from experiment, the trends are replicated to a reasonable level, and the discrepancies can be ascribed to errors in the fitted kinetic parameters, or the experimental data collection capabilities.[9]

Inspection of the reaction kinetics used in the model (see **Section S2**)[12,34] reveals how the partial current density for each product depends on the local pH and CO_2 concentration. Consistent with both experimental and theoretical studies,[4,5,11,12,35,36] the partial current densities for all CO_2R products exhibit an approximately first order dependence on the local CO_2 concentration under the assumption of low surface coverage by all adsorbed species. This assumption is supported by *operando* vibrational spectroscopy during CO_2R, which shows no signals for adsorbed intermediates during static elecrolysis.[37] Therefore, at a constant potential vs. SHE, increasing the local concentration of CO_2 will increase partial current densities for all CO_2-derived products about equally but have no effect on the partial current density for H_2

formation. Consequently, with increasing local concentration of CO_2, the FE for H_2 will decrease, but the relative ratio of FEs for C_1 and C_{2+} will remain relatively unchanged due to their similar orders in the concentration of CO_2. Regarding pH, the C_1 products and H_2 current densities have activation energies dependent on pH on the SHE scale.[4,11,12] When the pH increases, the current densities for both C_1 and H_2 products decrease relative to the current densities for C_{2+} products.

Additional insights into the manner that pulsed electrolysis contributes to the observed changes in product distribution can be obtained by examining a simulation for the start-up transient that leads to static electrolysis. **Figure 2C** illustrates the simulated start-up transient when the cathode voltage is suddenly reduced to $\Phi_2 = -1.55$ V vs SHE. This figure shows that a transient condition of pH and CO_2 concentration can be accessed at the onset of the transient that is not accessible under steady-state conditions. Within the first second, a high local concentration of CO_2 is attained, which, as noted above, significantly enhances the current density for CO_2R and suppresses H_2 evolution. This high current density rapidly boosts the surface pH, shifting the C_{2+} FE to a transient maximum that declines slightly as the CO_2 is depleted at the surface and the current density falls to its static value. Hence, by applying a pulsed potential signal, a transient maximum C_{2+} FE can be repeatedly realized as shown above in **Figure 1C** and **Section S6**. This phenomenon enables increased C_{2+} partial current densities when compared to static electrolysis at the time-averaged potential. The impacts of pH and CO_2 on C_{2+} product formation can be further appreciated by comparing their time-averaged values to those of static electrolysis. Pulsed electrolysis enables higher pH than every scenario except for static electrolysis at the more cathodic potential and enables a CO_2 concentration at the cathode surface only slightly

reduced when compared to static electrolysis at the time-averaged potential. These effects become more apparent when considering charge weighted time-averaging (see **Section S7**), which more heavily weights portions of the pulse where more current is passed to better represent the state of the electrode surface associated with the electrolysis. Based on this analysis, the pulsed signal possesses a charge-weighted, time-averaged potential of −1.52 V vs. SHE, surface pH of 10.93, and surface CO_2 concentration of 8.5 mM. This transient state is not achievable under conditions of static electrolysis, and helps explain the observed enhancements in current density and C_{2+} FE.

The transient analysis above elucidates a further area of improvement in the model. While the assumption of a low coverage of adsorbed CO has been demonstrated for static electrolysis,[37] it is possible that the transient state of high current density and CO_2 concentration observed at the beginning of the pulse causes the low-coverage assumption to no longer be valid, and a high coverage of adsorbed CO would further suppress the formation of H_2. This idea might explain the discrepancy between the H_2 FE for simulated and experimental pulsed electrolysis. We note, however, that capturing these effects requires a complete microkinetic model, and the kinetics used here demonstrate that a significant portion of the enhancements observed for pulsed electrolysis can be ascribed to the combined transient effects of enhanced CO_2 concentration and pH.

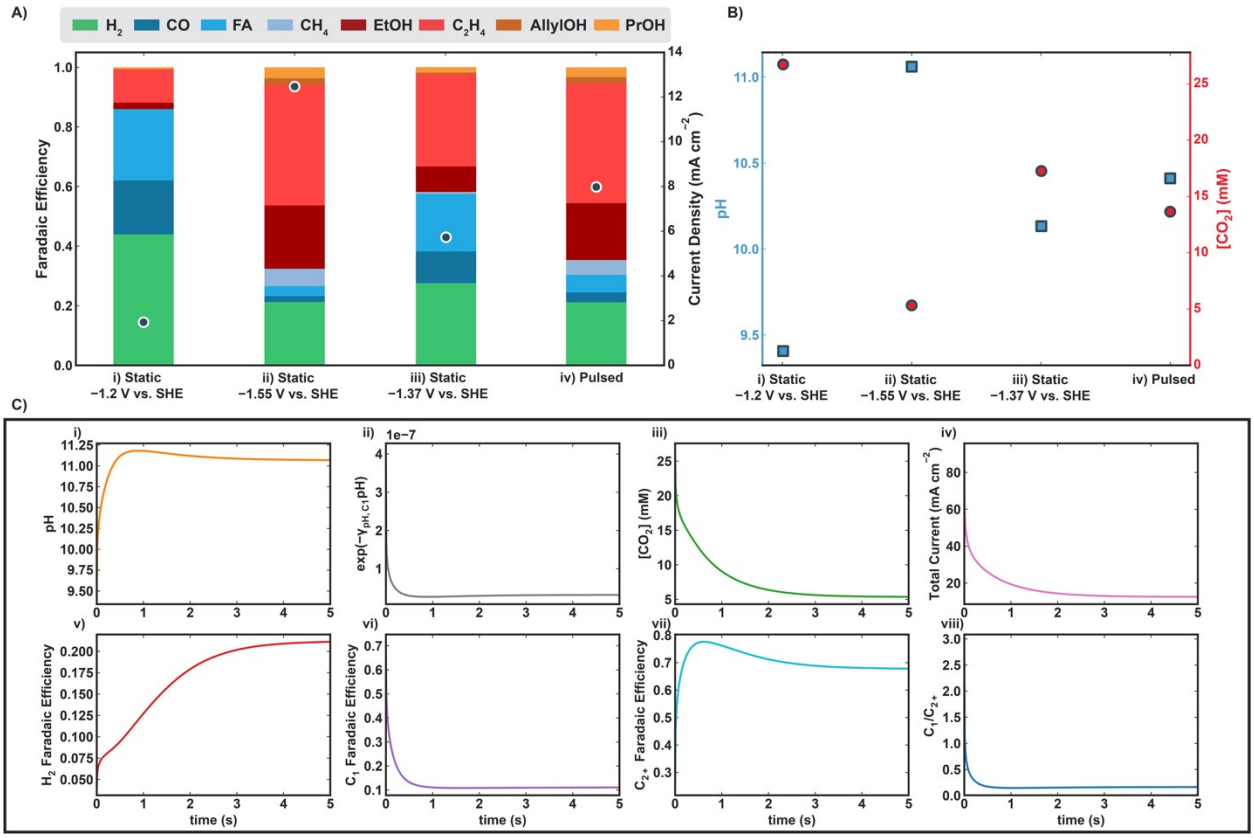

Figure 2: **(A)** Comparison of FEs (stacked bars) and current densities (markers) of static electrolysis at the **(i)** less cathodic, **(ii)** more cathodic, and **(iii)** time-averaged potentials to those in **(iv)** pulsed electrolysis where $\Phi_1 = -1.20$ V vs SHE and $\Phi_2 = -1.55$ V vs SHE, and $t_1 = t_2 = 10$ s. **(B)** Comparison of local pH during static electrolysis at the **(i)** less cathodic, **(ii)** more cathodic, and **(iii)** time-averaged potentials to time-averaged pH in **(iv)** pulsed electrolysis. **(C)** Transient start-up behavior of static electrolysis at $\Phi_2 = -1.55$ V vs SHE. **(i)** Surface pH, **(ii)** C_1 product formation pH dependence, **(iii)** surface CO_2 concentration, and **(iv)** total current density. **(v)** Faradaic efficiency of H_2, **(vi)** C_1 products, and **(vii)** C_{2+} products. **(viii)** Ratio of C_1 to C_{2+} product current densities.

The rate of mass transfer to and from the cathode surface is also known to affect the rate of CO_2R and the distribution of products formed. Our model captures the influence of mass-transfer through the choice of the boundary-layer thickness. As the boundary-layer thickness decreases, the rate of CO_2 mass transfer to the cathode increases, as does the rate of OH^- mass transfer from the cathode.[6,38,39] By changing the boundary-layer thicknesses under conditions of static electrolysis, it is possible to discern how mass transfer impacts the pH and the CO_2 concentration at the cathode and, in turn, the total current density and the distribution of

products. As shown in **Figure 3b-c** and **Figure S8,** decreasing the boundary-layer thickness increases the surface CO_2 concentration while maintaining the pH relatively constant. These changes can be rationalized in the following way. The increased flux of CO_2 that occurs upon reducing the boundary-layer thickness increases the local concentration of CO_2 at the cathode. The increased CO_2 concentration increases the CO_2R current density (due the positive order dependence on CO_2 concentration for all reactions that produce C-containing products). The rate of OH^- generation is also enhanced but is offset by the improved transport away from the electrode surface. The net effect of these changes is to decrease the FE for H_2 generation, as can be seen in **Figure 3a**. However, there is no notable improvement in the ratio of C_{2+}/C_1 products because the pH remains basically the same. These results are consistent with the findings of prior studies in which the boundary layer thickness was reduced by increasing the flowrate of CO_2 through the electrolyte or the supply of CO_2 to the cathode was increased by increasing the partial pressure of CO_2.[4,39–41]

By contrast, pulsed electrolysis results in an increase of about 0.3 of a pH unit (about a 2-fold increase in the OH^- concentration) near the cathode and about a 20% decrease in the local concentration of CO_2. As shown in Figure 3A, these effects lead to a suppression in the FE for the HER and increase in the FE for the CO_2R. This analysis further demonstrates that the changes in observed product distribution seen in pulsed electrolysis are due to the effects of both local pH and CO_2 concentration and not only the latter, as had been proposed earlier.[21] The simulations reported here clearly demonstrate that increases in pH drive the improvement in the ratio of C_{2+}/C_1 products and to the reduction in the FE for HER relative to CO_2R.

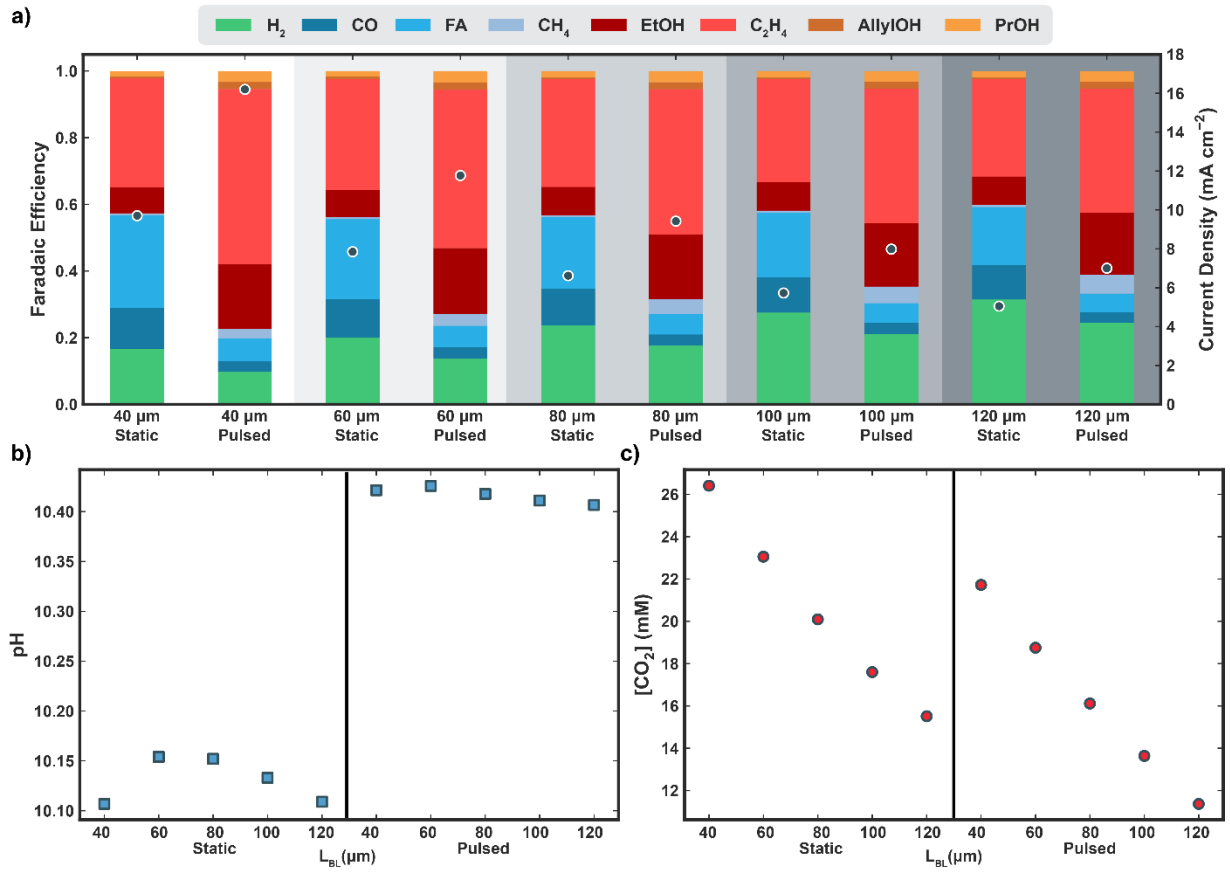

Figure 3: (a) Effect of mass-transfer boundary-layer thickness on FE (stacked bars) and total current density (markers) for static electrolysis and pulsed CO_2 electrolysis with Φ_1 = -1.55 V vs. SHE, Φ_2 = -1.2 V vs. SHE, and $t_1 = t_2 = 10$ s. Impact of boundary-layer thickness on **(b)** surface pH and **(c)** surface CO_2 concentration for pulsed and static electrolysis.

Another way to deconvolute the effects of pH and local CO_2 concentration on pulsed CO_2R is to examine the effects of electrolyte concentration (see **Section S10**). For higher concentrations of the $CsHCO_3$, the local pH rise at the Cu surface is mitigated for both pulsed and static electrolysis (**Figure S10b**) due to the enhanced buffering capacity of the electrolyte. As expected, the time-averaged local CO_2 concentration is lowered to maintain equilibrium with the carbonate species (**Figure S10c**). Furthermore, as prior analysis of the kinetics has shown, lower pH and local CO_2 concentration result in a significantly reduced C_{2+} selectivity, particularly for buffer concentrations > 1 M (**Figure S10a**). More interestingly, when a pulsed potential is applied to a system with a concentrated buffer electrolyte, the model predicts

exceptionally high selectivity to CH_4. This result is consistent with prior experimental studies for pulsed CO_2R on Cu that demonstrated improved CH_4 selectivity with increasing buffer electrolyte concentration.[42] The transient microenvironment accessed by pulsing a highly concentrated buffer solution is one of high CO_2 concentration, high overpotential, and low pH. These conditions are ideal for CH_4 formation, which primarily occurs at high overpotentials and is enhanced by the higher proton activities at low pHs. Therefore, pulsing provides a significant (~40-fold increase for 5 M $CsHCO_3$) enhancement in the selectivity of CH_4 under these conditions.

The model can also guide the selection of the ideal pulse characteristics for CO_2R. **Figure 4a** demonstrates that increased pulse amplitude leads to increased current density. It is also observed that CH_4 FE becomes significantly enhanced at higher amplitudes as result of its increased FE at high overpotentials as observed in static electrolysis.[4,12,21] Therefore, the intermediate cathodic potential, Φ_1 = -1.55 V vs. SHE, provides an optimal operating potential. Additionally, **Figure 4b** shows that a shorter pulse width leads to greater current density and C_{2+} FE. This result further demonstrates the importance of repeated access to the previously described transient. As the pulse width decreases, the fraction of time spent in the state of increased pH, CO_2, and overpotential is increased, improving performance. It is important to note, however, that this enhancement will eventually be limited by double-layer charging, because for shorter pulses (< 1 s), the current density will become dominated by double-layer charging as opposed to CO_2R.[19,26]

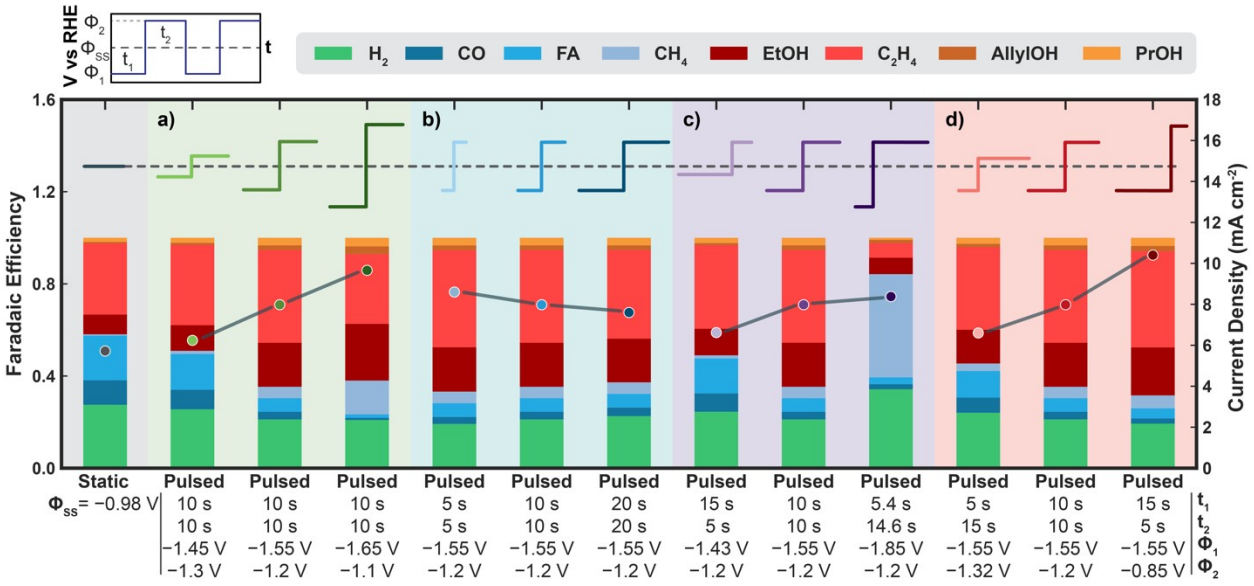

Figure 4: Effect of pulse characteristics on pulsed CO_2 electrolysis on FE (stacked bars) and total current density (markers). **(a)** Impact of pulse amplitude, **(b)** pulse width, **(c)** more cathodic potential, and **(d)** less cathodic potential at constant time-averaged potential (Φ_{SS} = -1.37 V vs. SHE). **Upper left inset**: Generalized voltage signal with labels for t_1 (the more cathodic duration), t_2 (the less cathodic duration), Φ_1 (the more cathodic pulse potential), Φ_2 (the less cathodic pulse potential), and Φ_{SS} (the steady-state potential). **Insets** depict various pulse shapes. See **Section S11** for transient profiles for each pulse shape.

Lastly, the impact of duty cycle at a constant vertex potential (**Figure 4c-d**) was evaluated. In these simulations, the duty cycle was modulated while maintaining one of the vertex potentials at the same time-averaged potential. As expected, the current density increases when the magnitude of the more cathodic potential increases (**Figure 4c**). However, Φ_1 = -1.55 V vs. SHE was found to be optimal for maximizing C_{2+} FE for the same reasons outlined above in the discussion of pulse amplitude. The highest current density and C_{2+} FE of any pulse shape was achieved by minimizing the less cathodic duty cycle at the optimal more cathodic potential of Φ_1 = -1.55 V vs. SHE (**Figure 4d**). This effect seems to be primarily driven by the reduced time and more positive potential at the less cathodic vertex limiting the amount of current passed during a state of low overpotential and pH, amplifying the charge-averaged potential and pH (see **Section S12**). However, this enhancement is also limited because at more positive cathodic

potentials, Cu oxidation can occur, as well as the oxidation of the formed CO_2R products.[21] It is important to note that the pulse shapes explored are a subset of those possible and the ones suggested are only the best amongst those studied, but this analysis demonstrates key trends and cements the importance of achieving states of maximum pH, CO_2 concentration, and overpotential to enhance C_{2+} FE.

Pulsed electrolysis has been demonstrated to improve the FE of C_{2+} products, but the cause of these improvements has not been properly understood. In this study, a multiphysics model of pulsed CO_2 electrolysis was developed that agrees with experimental trends and deconvolutes the effects of pH and CO_2 concentration on the kinetics of CO_2R. This work demonstrates that enhancements in C_{2+} FE observed for pulsed electrolysis are primarily driven by accessing to transient state of high pH, CO_2 concentration, and overpotential, and not solely due to a high CO_2 concentration, as suggested previously.[21] Furthermore, the ideal pulse shape is one for which the more cathodic potential is held around -1.55 V vs. SHE to increase pH without entering a regime of high CH_4 selectivity, and the less cathodic pulse duration and overpotential are both minimized to allow for improved access to the aforementioned enhanced state. The work also identifies areas for improving the accuracy of the model, especially at time scales where coverage effects and double-layer formation are relevant. In summary, the results of the present study provide insights to CO_2R that further clarify the role that the microenvironment at the cathode plays in dictating the observed FE and performance of CO_2R on Cu.

Acknowledgements

This material is based upon work performed at the Joint Center for Artificial Photosynthesis, a DOE Energy Innovation Hub, supported through the Office of Science of the U.S. Department of Energy under Award Number DE-SC0004993 and the National Institutes of Health under Grant No. S10OD023532. JCB acknowledges funding from the National Science Foundation Graduate Research Fellowship under Grant No. DGE 1752814. JCB would also like to acknowledge fruitful discussion regarding CO_2 reduction kinetics on copper surfaces with Joe Gauthier, Lalit Pant, and Kaitlin Corpus.

Associated Content

Supporting Information

The Supporting Information is available free of charge on the ACS Publications website at DOI: XXXX

Description of modeled physics, Description of modeled electrode kinetics for CO_2R, Computational methods, Experimentally observed current density and CO_2 concentration, Additional data for pulsed simulation, Transient data for pulsed simulation, Charge-weighted time averaging for local pH and CO_2 concentration, Impact of boundary layer thickness on local OH^- concentration, Time-dependent potential, surface pH, and surface CO_2 concentration for various mass-transport boundary layer thicknesses, Impact of buffer concentration on static and pulsed CO_2 electrolysis, Time-dependent potential, surface pH, and surface CO_2 concentration for various pulse shapes, Charge-weighted time averages for optimal pulse shape.

References

(1) Resasco, J.; Bell, A. T. Electrocatalytic CO2 Reduction to Fuels: Progress and Opportunities. *Trends Chem.* **2020**, *2* (9), 825–836. https://doi.org/10.1016/j.trechm.2020.06.007.

(2) Garg, S.; Li, M.; Weber, A. Z.; Ge, L.; Li, L.; Rudolph, V.; Wang, G.; Rufford, T. E. Advances and Challenges in Electrochemical CO2 Reduction Processes: An Engineering and Design Perspective Looking beyond New Catalyst Materials. *J. Mater. Chem. A* **2020**, *8* (4), 1511–1544. https://doi.org/10.1039/c9ta13298h.

(3) Fan, L.; Xia, C.; Yang, F.; Wang, J.; Wang, H.; Lu, Y. Strategies in Catalysts and Electrolyzer Design for Electrochemical CO2 Reduction toward C2+ Products. *Sci. Adv.* **2020**, *6* (8), 1–18. https://doi.org/10.1126/sciadv.aay3111.

(4) Wang, L.; Nitopi, S. A.; Bertheussen, E.; Orazov, M.; Morales-Guio, C. G.; Liu, X.; Higgins, D. C.; Chan, K.; Nørskov, J. K.; Hahn, C.; Jaramillo, T. F. Electrochemical Carbon Monoxide Reduction on Polycrystalline Copper: Effects of Potential, Pressure, and pH on Selectivity toward Multicarbon and Oxygenated Products. *ACS Catal.* **2018**, *8* (8), 7445–7454. https://doi.org/10.1021/acscatal.8b01200.

(5) Nitopi, S.; Bertheussen, E.; Scott, S. B.; Liu, X.; Engstfeld, A. K.; Horch, S.; Seger, B.; Stephens, I. E. L.; Chan, K.; Hahn, C.; Nørskov, J. K.; Jaramillo, T. F.; Chorkendorff, I. Progress and Perspectives of Electrochemical CO2 Reduction on Copper in Aqueous Electrolyte. *Chem. Rev.* **2019**, *119* (12), 7610–7672. https://doi.org/10.1021/acs.chemrev.8b00705.

(6) Clark, E. L.; Resasco, J.; Landers, A.; Lin, J.; Chung, L. T.; Walton, A.; Hahn, C.; Jaramillo, T. F.; Bell, A. T. Standards and Protocols for Data Acquisition and Reporting for Studies of the Electrochemical Reduction of Carbon Dioxide. *ACS Catal.* **2018**, *8* (7), 6560–6570. https://doi.org/10.1021/acscatal.8b01340.

(7) Hahn, C.; Jaramillo, T. F. Using Microenvironments to Control Reactivity in CO2 Electrocatalysis. *Joule* **2020**, *4* (2), 292–294. https://doi.org/10.1016/j.joule.2020.01.017.

(8) Singh, M. R.; Clark, E. L.; Bell, A. T. Effects of Electrolyte, Catalyst, and Membrane Composition and Operating Conditions on the Performance of Solar-Driven Electrochemical Reduction of Carbon Dioxide. *Phys. Chem. Chem. Phys.* **2015**, *17* (29), 18924–18936. https://doi.org/10.1039/c5cp03283k.

(9) Bohra, D.; Chaudhry, J. H.; Burdyny, T.; Pidko, E. A.; Smith, W. A. Modeling the Electrical Double Layer to Understand the Reaction Environment in a CO2 Electrocatalytic System. *Energy Environ. Sci.* **2019**, *12* (11), 3380–3389. https://doi.org/10.1039/c9ee02485a.

(10) Zhang, Z.; Melo, L.; Jansonius, R. P.; Habibzadeh, F.; Grant, E. R.; Berlinguette, C. P. PH Matters When Reducing CO2in an Electrochemical Flow Cell. *ACS Energy Lett.* **2020**, *5* (10), 3101–3107. https://doi.org/10.1021/acsenergylett.0c01606.

(11) Hori, Y.; Takahashi, R.; Yoshinami, Y.; Murata, A. Electrochemical Reduction of CO at a Copper Electrode. *J. Phys. Chem. B* **1997**, *101* (36), 7075–7081. https://doi.org/10.1021/jp970284i.

(12) Liu, X.; Schlexer, P.; Xiao, J.; Ji, Y.; Wang, L.; Sandberg, R. B.; Tang, M.; Brown, K. S.; Peng, H.; Ringe, S.; Hahn, C.; Jaramillo, T. F.; Nørskov, J. K.; Chan, K. PH Effects on the Electrochemical Reduction of CO (2) towards C 2 Products on Stepped Copper. *Nat. Commun.* **2019**, *10* (1), 1–10. https://doi.org/10.1038/s41467-018-07970-9.

(13) Weng, L. C.; Bell, A. T.; Weber, A. Z. A Systematic Analysis of Cu-Based Membrane-Electrode Assemblies for CO2reduction through Multiphysics Simulation. *Energy Environ. Sci.* **2020**, *13* (10), 3592–3606. https://doi.org/10.1039/d0ee01604g.

(14) García de Arquer, F. P.; Dinh, C. T.; Ozden, A.; Wicks, J.; McCallum, C.; Kirmani, A. R.; Nam, D. H.; Gabardo, C.; Seifitokaldani, A.; Wang, X.; Li, Y. C.; Li, F.; Edwards, J.; Richter, L. J.; Thorpe, S. J.; Sinton, D.; Sargent, E. H. CO2 Electrolysis to Multicarbon Products at Activities Greater than 1 A Cm−2. *Science (80-.).* **2020**, *367* (6478), 661–666. https://doi.org/10.1126/science.aay4217.

(15) Cui, Y.; He, B.; Liu, X.; Sun, J. Ionic Liquids-Promoted Electrocatalytic Reduction of Carbon Dioxide. *Ind. Eng. Chem. Res.* **2020**, *59* (46), 20235–20252. https://doi.org/10.1021/acs.iecr.0c04037.

(16) Han, Z.; Kortlever, R.; Chen, H. Y.; Peters, J. C.; Agapie, T. CO2 Reduction Selective for C ≥ 2 Products on Polycrystalline Copper with N-Substituted Pyridinium Additives. *ACS Cent. Sci.* **2017**, *3* (8), 853–859. https://doi.org/10.1021/acscentsci.7b00180.

(17) Nam, D. H.; De Luna, P.; Rosas-Hernández, A.; Thevenon, A.; Li, F.; Agapie, T.; Peters, J. C.; Shekhah, O.; Eddaoudi, M.; Sargent, E. H. Molecular Enhancement of Heterogeneous CO2 Reduction. *Nat. Mater.* **2020**, *19* (3), 266–276. https://doi.org/10.1038/s41563-020-0610-2.

(18) Lum, Y.; Ager, J. W. Sequential Catalysis Controls Selectivity in Electrochemical CO2 Reduction on Cu. *Energy Environ. Sci.* **2018**, *11* (10), 2935–2944. https://doi.org/10.1039/c8ee01501e.

(19) Kimura, K. W.; Fritz, K. E.; Kim, J.; Suntivich, J.; Abruña, H. D.; Hanrath, T. Controlled Selectivity of CO2 Reduction on Copper by Pulsing the Electrochemical Potential. *ChemSusChem* **2018**, *11* (11), 1781–1786. https://doi.org/10.1002/cssc.201800318.

(20) Engelbrecht, A.; Uhlig, C.; Stark, O.; Hämmerle, M.; Schmid, G.; Magori, E.; Wiesner-Fleischer, K.; Fleischer, M.; Moos, R. On the Electrochemical CO 2 Reduction at Copper Sheet Electrodes with Enhanced Long-Term Stability by Pulsed Electrolysis . *J. Electrochem. Soc.* **2018**, *165* (15), J3059–J3068. https://doi.org/10.1149/2.0091815jes.

(21) Kim, C.; Weng, L. C.; Bell, A. T. Impact of Pulsed Electrochemical Reduction of CO2 on the Formation of C2+Products over Cu. *ACS Catal.* **2020**, *10* (21), 12403–12413. https://doi.org/10.1021/acscatal.0c02915.

(22) Shiratsuchi, R.; Aikoh, Y.; Nogami, G. Pulsed Electroreduction of CO 2 on Copper Electrodes. *J. Electrochem. Soc.* **1993**, *140* (12), 3479–3482. https://doi.org/10.1149/1.2221113.

(23) Yano, J.; Yamasaki, S. Pulse-Mode Electrochemical Reduction of Carbon Dioxide Using Copper and Copper Oxide Electrodes for Selective Ethylene Formation. *J. Appl. Electrochem.* **2008**, *38* (12), 1721–1726. https://doi.org/10.1007/s10800-008-9622-3.

(24) Arán-Ais, R. M.; Scholten, F.; Kunze, S.; Rizo, R.; Roldan Cuenya, B. The Role of in Situ Generated Morphological Motifs and Cu(i) Species in C2+ Product Selectivity during CO2 Pulsed Electroreduction. *Nat. Energy* **2020**, *5* (4), 317–325. https://doi.org/10.1038/s41560-020-0594-9.

(25) Kimura, K. W.; Casebolt, R.; Cimada Dasilva, J.; Kauffman, E.; Kim, J.; Dunbar, T. A.; Pollock, C. J.; Suntivich, J.; Hanrath, T. Selective Electrochemical CO2Reduction during Pulsed Potential Stems from Dynamic Interface. *ACS Catal.* **2020**, *10* (15), 8632–8639. https://doi.org/10.1021/acscatal.0c02630.

(26) Strain, J. M.; Gulati, S.; Pishgar, S.; Spurgeon, J. M. Pulsed Electrochemical Carbon Monoxide Reduction on Oxide-Derived Copper Catalyst. *ChemSusChem* **2020**, *13* (11), 3028–3033. https://doi.org/10.1002/cssc.202000464.

(27) Newman, J.; Thomas-Alyea, K. E. *Electrochemical Systems*, 3rd ed.; John Wiley and Sons, Inc.: Hoboken, NJ, 2004.

(28) Press, C. *CRC Handbook of Chemistry and Physics*; Cleveland, Ohio, 1977.

(29) Weng, L. C.; Bell, A. T.; Weber, A. Z. Towards Membrane-Electrode Assembly Systems for CO2 Reduction: A Modeling Study. *Energy Environ. Sci.* **2019**, *12* (6), 1950–1968. https://doi.org/10.1039/c9ee00909d.

(30) Weng, L. C.; Bell, A. T.; Weber, A. Z. A Systematic Analysis of Cu-Based Membrane-Electrode Assemblies for CO2reduction through Multiphysics Simulation. *Energy Environ. Sci.* **2020**, *13* (10), 3592–3606. https://doi.org/10.1039/d0ee01604g.

(31) Yang, K.; Kas, R.; Smith, W. A. In Situ Infrared Spectroscopy Reveals Persistent Alkalinity near Electrode Surfaces during CO2 Electroreduction. *J. Am. Chem. Soc.* **2019**, *141* (40). https://doi.org/10.1021/jacs.9b07000.

(32) Ebaid, M.; Jiang, K.; Zhang, Z.; Drisdell, W. S.; Bell, A. T.; Cooper, J. K. Production of C 2 /C 3 Oxygenates from Planar Copper Nitride-Derived Mesoporous Copper via Electrochemical Reduction of CO 2 . *Chem. Mater.* **2020**, *32* (7), 3304–3311. https://doi.org/10.1021/acs.chemmater.0c00761.

(33) Härtinger, S.; Doblhofer, K. The Electrochemical Interface between Copper(111) and Aqueous Electrolytes. *J. Electroanal. Chem.* **1995**, *380* (1–2), 185–191. https://doi.org/10.1016/0022-0728(94)03650-R.

(34) Weng, L. C.; Bell, A. T.; Weber, A. Z. Modeling Gas-Diffusion Electrodes for CO2 Reduction. *Phys. Chem. Chem. Phys.* **2018**, *20* (25), 16973–16984.

https://doi.org/10.1039/c8cp01319e.

(35) Li, J.; Wang, Z.; McCallum, C.; Xu, Y.; Li, F.; Wang, Y.; Gabardo, C. M.; Dinh, C. T.; Zhuang, T. T.; Wang, L.; Howe, J. Y.; Ren, Y.; Sargent, E. H.; Sinton, D. Constraining CO Coverage on Copper Promotes High-Efficiency Ethylene Electroproduction. *Nat. Catal.* **2019**, *2* (12), 1124–1131. https://doi.org/10.1038/s41929-019-0380-x.

(36) Zhang, T.; Li, Z.; Zhang, J.; Wu, J. Enhance CO2-to-C2+ Products Yield through Spatial Management of CO Transport in Cu/ZnO Tandem Electrodes. *J. Catal.* **2020**, *387*, 163–169. https://doi.org/10.1016/j.jcat.2020.05.002.

(37) Dunwell, M.; Luc, W.; Yan, Y.; Jiao, F.; Xu, B. Understanding Surface-Mediated Electrochemical Reactions: CO2 Reduction and Beyond. *ACS Catal.* **2018**, *8* (9), 8121–8129. https://doi.org/10.1021/acscatal.8b02181.

(38) Bird, B. R.; Stewart, W. E.; Edwin, N. L. *Transport Phenomena*, 2nd ed.; Wiley: Danvers, MA, 2007.

(39) Clark, E. L.; Bell, A. T. Direct Observation of the Local Reaction Environment during the Electrochemical Reduction of CO2. *J. Am. Chem. Soc.* **2018**, *140* (22), 7012–7020. https://doi.org/10.1021/jacs.8b04058.

(40) Hara, K.; Tsuneto, A.; Kudo, A.; Sakata, T. Electrochemical Reduction of CO 2 on a Cu Electrode under High Pressure: Factors That Determine the Product Selectivity. *J. Electrochem. Soc.* **1994**, *141* (8), 2097–2103. https://doi.org/10.1149/1.2055067.

(41) Gupta, N.; Gattrell, M.; MacDougall, B. Calculation for the Cathode Surface Concentrations in the Electrochemical Reduction of CO2 in KHCO3 Solutions. *J. Appl. Electrochem.* **2006**, *36* (2), 161–172. https://doi.org/10.1007/s10800-005-9058-y.

(42) Casebolt, R.; Kimura, K. W.; Levine, K.; Cimada DaSilva, J. A.; Kim, J.; Dunbar, T. A.; Suntivich, J.; Hanrath, T. Effect of Electrolyte Composition and Concentration on Pulsed Potential Electrochemical CO2 Reduction. *ChemElectroChem* **2020**, 681–688. https://doi.org/10.1002/celc.202001445.

For Table of Contents Only